CHEMISTRY OF MATERIALS
Article

Chem. Mater. **2010,** *22,* 1015–1021 1015
DOI:10.1021/cm9018309

Coprecipitation Synthesis of $Ni_xMn_{1-x}(OH)_2$ Mixed Hydroxides†

Fu Zhou,‡ Xuemei Zhao,‡ Andrew van Bommel,§ Aaron W. Rowe,§ and J. R. Dahn*,‡

‡*Department of Physics and Atmospheric Science, Dalhousie University, Halifax, N.S., B3H 3J5, Canada, and* §*Department of Chemistry, Dalhousie University, Halifax, N.S., B3H 3J5, Canada*

Received June 27, 2009. Revised Manuscript Received October 14, 2009

Four separate coprecipitation routes were applied to the preparation of $Ni_xMn_{1-x}(OH)_2$ mixed hydroxides with $x = 1$, 5/6, 2/3, 1/2, 1/3, and 0, beginning with divalent nitrates. The structure and morphology of the samples were studied by X-ray diffraction and scanning electron microscopy techniques. Intentionally bubbled air during coprecipitation was found to create layered double hydroxide (LDH) phases for $x = 5/6$, coexisting LDH and Mn_3O_4 phases for $5/6 > x > 0$, and Mn_3O_4 for $x = 0$. On the basis of the structures observed, these trends could be attributed to the relative ease of oxidation of Mn^{2+} to Mn^{3+}. Pure hydroxides, with the expected $Ni(OH)_2$ structure, were prepared for all x when air was excluded from the coprecipitation reaction. Spherical and dense particles could be prepared for all compositions attempted when ammonia was added during coprecipitation under anaerobic conditions.

Introduction

Layered lithium transition metal oxide compositions $Li[Ni_xMn_{1-x}]O_2$ have been reported to be promising positive electrode materials as possible replacements for $LiCoO_2$ because of their high capacity, good capacity retention, low toxicity, and lower raw material cost.[1−4] The most common synthesis method for these oxides is the mixed hydroxide method that consists of two steps.[1] The first step is a coprecipitation of mixed transition metal salts in a stirred solution of LiOH or NaOH, which is thought to cause the precipitation of $M(OH)_2$ (M = Ni and Mn) with a uniform cation distribution. The second step consists of mixing the $M(OH)_2$ with a stoichiometric amount of $LiOH \cdot H_2O$ or Li_2CO_3 and heating the mixture in air at high temperature.

Previous research has suggested that the particle size and morphology of the final oxide products, which impacts the physical and electrochemical properties of the positive electrode materials, is strongly affected by the properties of the intermediate mixed hydroxides.[5−7] Thus, to get positive electrode materials with excellent electrochemical properties, the coprecipitation synthesis of the mixed hydroxide intermediate phases must be thoroughly studied and understood. Mixed hydroxide intermediates with appropriate chemistry, size, and morphology must be prepared. Many authors of studies on lithium transition metal oxides that use the mixed hydroxide method never report the structure and properties of the hydroxide intermediates that they prepare. One goal of this paper is to demonstrate the wide variety of materials that can be prepared depending on x in the $Ni_xMn_{1-x}(OH)_2$ target phase and on the coprecipitation conditions. Then, other research groups can compare their conditions to the ones considered here and learn what type of intermediate phase (or phases) preferentially forms.

In the preparation of $Ni_xMn_{1-x}(OH)_2$ targets, the presence of Mn is expected to be problematic because Mn^{2+} cations can be easily oxidized to Mn^{3+} cations. The presence of cations with an oxidation state of +3 causes the formation of other phases as we have demonstrated in our previous research.[8,9] The as-prepared intermediates change from single phase $M(OH)_2$ into two-phase products of $M(OH)_2$ and layered double hydroxide (LDH), where the cation distribution may not be the same in the two phases. The LDH phases incorporate intercalated NO_3^-, CO_3^{2-}, or SO_4^{2-} anions to compensate the charge of the 3+ cations. These anions are released as toxic gases during the second step of the oxide production, which can be problematic in developed countries during industrial scale synthesis. Furthermore, when x is small, the possibility of the formation of M_3O_4 spinel, which incorporates Mn^{3+}, exists. Measures that successfully prevent cations, especially Mn, from oxidation during the coprecipitation process need to be established.

† Accepted as part of the 2010 "Materials Chemistry of Energy Conversion Special Issue".

*Corresponding author e-mail: jeff.dahn@dal.ca.

(1) Ohzuku, T.; Makimura, Y. *Chem. Lett.* **2001**, *8*, 744.
(2) Makimura, Y.; Ohzuku, T. *J. Power Sources* **2003**, *119*, 156.
(3) Zhang, X.; Wen, Z.; Zhu, X.; Lin, B.; Zhang, J.; Huang, S. *Mater. Lett.* **2006**, *60*, 1470.
(4) Kang, S.; Kim, J.; Stoll, M.; Abraham, D.; Sun, Y.; Amine, K. *J. Power Sources* **2002**, *112*, 41.
(5) Lee, K.; Myung, S.; Moon, J.; Sun, Y. *Electrochim. Acta* **2008**, *53*, 6033.
(6) Bang, H.; Park, B.; Prakash, J.; Sun, Y. *J. Power Sources* **2007**, *174*, 565.
(7) Kim, G.; Myung, S.; Kim, H.; Sun, Y. *Electrochim. Acta* **2006**, *51*, 2447.
(8) Zhao, X.; Zhou, F.; Dahn, J. R. *J. Electrochem. Soc.* **2008**, *155*, A642.
(9) Luo, W.; Dahn, J. R. *Chem. Mater.* **2009**, *21*, 56.

Published on Web 11/04/2009

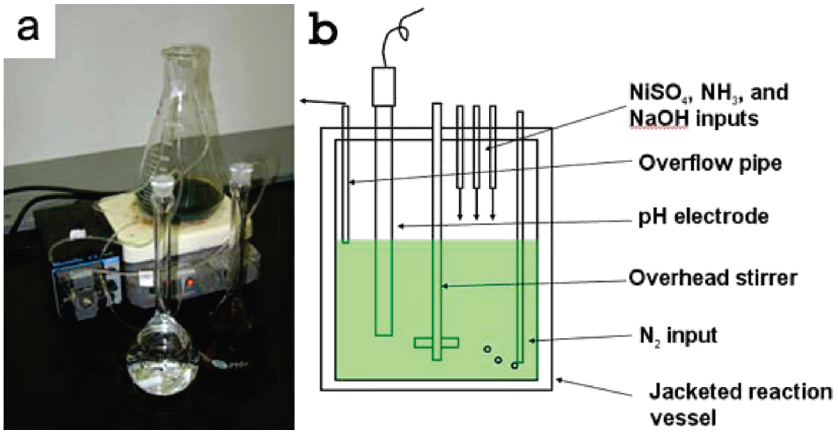

Figure 1. Small pump system (a) and schematic drawing of the continuous reactor system (b) used for the coprecipitation synthesis studies reported here.

Many different procedures have been reported on the coprecipitation synthesis of mixed hydroxides.[5−7,10−13] The numerous synthetic procedures lead to mixed hydroxide intermediates with variable structure, particle size, and morphology, which further leads to electrode materials with diverse electrochemical properties. However, the detailed structure and composition of the hydroxide intermediates have not been reported in a systematic way for a range of Ni:Mn ratios and for a range of synthesis conditions. It is hoped that this paper helps fill that gap.

Experimental Section

Reagents used in this investigation included nickel(II) nitrate hexahydrate (98%, Alfa Aesar), manganese nitrate tetrahydrate (98%, Alfa Aesar), $LiOH \cdot H_2O$ (Alfa Aesar), sodium hydroxide (Alfa Aesar), and ammonium hydroxide (28.0−30.0%, Sigma-Aldrich).

Figure 1 shows the two separate sets of equipment that were used for the coprecipitation reactions. Figure 1a shows a two-channel Masterflex C/L electronic metering pump that was used to simultaneously feed the mixed nitrate and sodium hydroxide solutions from the shown volumetric flasks to the shown stirred flask. Figure 1b shows a schematic drawing of a continuous reactor fitted with a 2 L jacketed reaction vessel. The reactor monitors and controls pH and temperature. The metal hydroxides were produced by the coprecipitation reaction between metal nitrates and NaOH with the addition of ammonia at a controlled PH.

Four different coprecipitation procedures were tested in our study as follows:

In route 1, the metal nitrates were dissolved in distilled water to obtain 1.00 L of a 2.00 M mixed metal nitrate solution, and sodium hydroxide was dissolved in distilled water to make 1 L of a 5.00 M NaOH solution. The coprecipitation experiment was carried out at room temperature in the continuous reactor by deliberately bubbling air (compressed air, containing normal amounts of N_2, O_2, and CO_2) into the reactor and without ammonia addition or pH control. After reaction, the products were filtered and washed several times with 3 L of distilled water by centrifuging. The rinsed products were dried in air at 80 °C overnight before X-ray diffraction (XRD) and scanning electron microscopy (SEM) tests.

In route 2, metal nitrates were dissolved in distilled water to obtain 250 mL of a 0.40 M mixed metal nitrate solution. A total of 250 mL of a 0.80 M lithium hydroxide solution was also prepared using distilled water. These solutions were simultaneously dripped into a stirred flask using the equipment shown in Figure 1a in 1 h. After the reaction, the products were filtered and rinsed several times by centrifuging with 3 L of distilled water. The rinsed products were dried in air at 80 °C overnight before XRD and SEM tests.

In route 3, the parameters were similar to those in route 2. Differences were that the solutions were prepared with deaerated distilled water (prepared by boiling for 15 min followed by immediate use) and that the solution concentrations were 2 M for the mixed metal nitrate and 4 M for the LiOH.

In route 4, all solutions were prepared with deaerated distilled water, and the continuous reactor (Figure 1b) was used. Reagents were added using digital peristaltic pumps (Masterflex L/S 07524), and sodium hydroxide addition was automatically controlled and added by the peristaltic pump on the reactor. Reaction contents were maintained at a temperature of 60 °C, and the contents of the reactor were stirred by an overhead stirrer at 1000 rpm. The pH meter and electrode (Mettler-Toledo InLab 424) were calibrated at 60 °C using buffer solutions. The pH values of the buffer solution were 7.0 at 60 °C (Fisher Scientific) and 11.1 at 60 °C (Fixanal, Riedel-de Haën). A volume of 1.00 L of a 1.00 M ammonia solution made in deaerated water was added to the continuous reactor and then heated to 60 °C. The reaction proceeded with the addition of 5.0 M ammonia at 0.005 L/h and 2.0 M MSO_4 at 0.035 L/h. A concentration of 5.0 M NaOH was automatically added to the reaction contents to maintain the desired pH value (assumed to be 0.02 L/h). The reaction vessel was fitted with an overflow pipe to ensure a constant volume during the reaction, and the reaction vessel was purged with nitrogen to exclude oxygen. The residence time, given by the total flow rate of the reagents and the reactor volume, was 20 h. The total reaction time was 40 h. After the reaction, the products were filtered and washed with 3 L of deaerated distilled water. The rinsed products were dried in air at 80 °C overnight before XRD and SEM tests. Table I lists the details of the four synthetic routes.

X-ray diffraction was made using a Siemens D5000 diffractometer equipped with a copper target X-ray tube and a diffracted beam monochromator. The divergence and antiscatter slits were both set to 0.5°, and the receiving slit was 0.2 mm. Data

(10) Li, H.; Chen, G.; Zhang, B.; Xu, J. *Solid State Commun.* **2008**, *146*, 115.
(11) Zhang, S. *Electrochim. Acta* **2007**, *52*, 7337.
(12) Luo, X.; Wang, X.; Liao, L.; Gamboa, S.; Sebastian, P. *J. Power Sources* **2006**, *158*, 654.
(13) Wu, S.; Yang, C. *J. Power Sources* **2005**, *146*, 270.

Table I. Detailed Synthetic Parameters of the Four Different Coprecipitation Routes for Synthesis of Ni_xMn_{1-x} Mixed Hydroxide Intermediates

route number	reactor used	atmosphere	solvent	metal nitrate solution concentration	LiOH or ammonia solution concentration	chelating agent	pH control	temperature control
1	continuous reactor (Figure 1b)	bubbling air	normal distilled water	2 mol/L	NaOH 4 mol/L	no	no	no
2	small pump system	static air	normal distilled water	0.4 mol/L	LiOH 0.8 mol/L	no	no	no
3	small pump system	static air	deaerated distilled water	2 mol/L	LiOH 4 mol/L	no	no	no
4	continuous reactor (Figure 1b)	N_2	deaerated distilled water	2 mol/L	NaOH 5 mol/L	ammonia 1 mol/L	9.8	60 °C

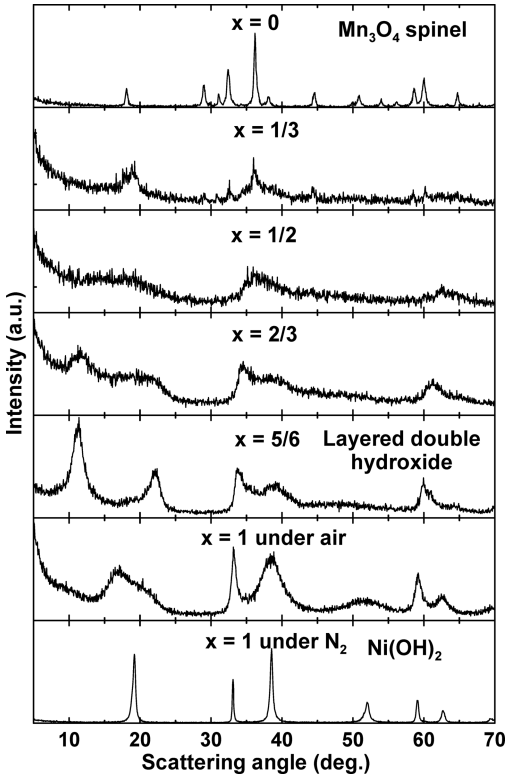

Figure 2. XRD patterns of the Ni_xMn_{1-x} mixed hydroxide samples with $x = 1, 5/6, 2/3, 1/2, 1/3$, and 0 synthesized using route 1. The bottom panel shows data for the $x = 1$ sample synthesized using route 4 under N_2.

was collected in 0.05° intervals in the scattering angle range between 5° and 70°. The count time was 5 s per point. CHN analysis was performed on the coprecipitated mixed hydroxide samples at Canadian Microanalytical Services in Delta, B.C., Canada. A Hitachi S-4700 SEM was used to study the particle size and morphology of the as-prepared products. Thermogravimetric analysis of the samples under air was made between room temperature and 800 °C using a TA Instruments SDT-600.

Results and Discussion

Figure 2 shows the XRD patterns of the targeted Ni_xMn_{1-x} mixed hydroxides with $x = 1$, 5/6, 2/3, 1/2, 1/3, and 0 synthesized using route 1. In addition, the XRD pattern of $Ni(OH)_2$ synthesized using route 4 is shown for comparison in the bottom panel of Figure 1. Instead of the expected $Ni_xMn_{1-x}(OH)_2$ phase, the obtained materials, synthesized in the presence of deliberately introduced air (route 1), are quite different. The materials with $x = 5/6$ and $x = 2/3$ show a strong diffraction peak near 11.5 degrees, which is indicative of large spacing between $M(OH)_2$ slabs. This results from the incorporation of anions to compensate the charge of 3+ cations incorporated into the materials due to oxidation caused by the synthesis in air. Such materials have the general formula $M_x^{2+}M_{1-x}^{3+}(OH)_2(A^{n-})_{(1-x)/n}$ and are called "layered double hydroxides (LDH)".[8] The material with $x = 5/6$ has a diffraction pattern that closely matches the pattern of the pure layered double hydroxide phase we have reported in the Al substituted Co_zAl_{1-z} mixed hydroxide series with $z = 0.2$.[9] The existence of the LDH phase for $x = 5/6$ and $x = 2/3$ indicates that some of the cations must have been oxidized from the +2 oxidation state to the +3 oxidation state. The (003) and (006) peaks of the LDH phase near 11.5° and 22°, respectively, indicate parallel stacking of the $M(OH)_2$ slabs. The (10 L) series of Bragg peaks is poorly formed, indicating that the layers are stacked with a significant degree of turbostratic misalignment.

The sample with $x = 1/2$ in Figure 2 shows a diffraction pattern with almost no evidence for the parallel stacking of $M(OH)_2$ slabs because the (00 L) peaks do not appear. All that remains are the (10) and (11) "two-dimensional peaks" consistent with the presence of single, or randomly stacked, $M(OH)_2$ slabs. Presumably, these slabs would have associated anions due to the presence of +3 cations. When $x = 1/3$, the pattern shows significant evidence for the formation of M_3O_4 spinel based on a comparison to the pattern for $x = 0$, which matches that of Mn_3O_4 as discussed below.

The top panel of Figure 2 shows the XRD pattern of the $x = 0$ product from the route 1 synthesis. In this case, only Mn^{2+} cations were used as the reagents. According to the Pourbaix diagram,[14] the possible products based on the conditions of our synthetic route could be Mn_2O_3 or Mn_3O_4. The $x = 0$ product displays typical diffraction peaks of Mn_3O_4 spinel phase. However, γ-Mn_2O_3 has a very similar crystal structure to Mn_3O_4 spinel.[14,15] To verify the product composition, we performed Rietveld refinement of the XRD powder pattern using the Rietica software.[16] Figure 3 shows the XRD pattern of the $x = 0$

(14) He, W.; Zhang, Y.; Zhang, X.; Wang, H.; Yan, H. *J. Cryst. Growth* **2003**, *252*, 285.
(15) Gui, Z.; Fan, R.; Chen, X.; Wu, Y. *Inorg. Chem. Commun.* **2001**, *4*, 294.
(16) (a) Hunter, B. Rietica: A Visual Rietveld Program, version 1.71; International Union of Crystallography, Commission on Powder Diffraction, **1998**; Windows version of LHPM, Newsletter No. 20. (b) Hill, R. J.; Howard, C. J. *J. Appl. Crystallogr.* **1985**, *18*, 173. (c) Wiles, D. B.; Young, R. A. *J. Appl. Crystallogr.* **1981**, *14*, 149.

product in the scattering angle range between 10°and 90° along with the Rietveld fit. The inset of Figure 3 is the Rietveld fit between 70° and 80° to demonstrate the quality of the Rietveld fit. Table II shows the lattice constants and oxygen occupancy of the product together with the associated errors. These parameters agree well with literature values for the Mn_3O_4 phase (JCPDS 24-0734). Therefore, we believe that the $x = 0$ sample synthesized in the presence of air (route 1) is Mn_3O_4 spinel.

Figure 2 shows the XRD patterns of the $x = 1$ products synthesized under air (route 1) and under nitrogen (route 4). When synthesizing under nitrogen (route 4), the pattern matches that of $Ni(OH)_2$. However, when air is deliberately forced into the solution, the pattern is quite different. In particular, the (001) peak, which is near 19° and sharp for $Ni(OH)_2$, appears broad and shifted to a lower scattering angle for the sample with $x = 1$ made by route 1. By contrast, the (100) and (110) peaks are sharp, while the (10 L) series of peaks is broad. These features are consistent with the presence of stacking faults and also the presence of some layers with an expanded layer spacing. We suggest that some Ni has been oxidized to Ni^{3+} and a corresponding number of NO_3^- or CO_3^{2-} anions (originating from the forced air) have been incorporated within some galleries between $Ni(OH)_2$ slabs in a random manner. This would lead to two different interslab distances and could broaden the (001) peak if the arrangement of the layers with different interslab distances were random.

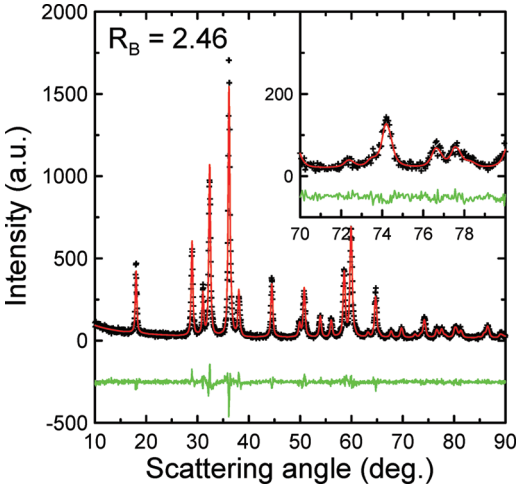

Figure 3. XRD pattern of the Ni_xMn_{1-x} mixed hydroxide with $x = 0$ synthesized using route 1 along with the Rietveld refinement showing that the sample is Mn_3O_4.

Table II. Lattice Constants and Oxygen Occupancy of the $x = 0$ Sample Synthesized through Route 1 on the Basis of the Mn_3O_4 Spinel Structure[a]

lattice constant, a (Å)	lattice constant, c (Å)	oxygen occupancy
5.765(5)	9.466(5)	4.120(5)

[a] Errors in the last digit are shown in brackets.

Figure 2 suggests that Mn is more easily oxidized than Ni on the basis of the complete conversion of the $x = 0$ sample to Mn_3O_4 in the presence of air. In our previous work on $Co_{1-x}Al_x(OH)_2(NO_3)_x$,[9] we showed that single-phase LDH phases could be prepared for x near 1/6. The diffraction pattern of the sample with $x = 5/6$ is a predominantly pure LDH phase. If all of the Mn in this material were oxidized to Mn^{3+}, and the more stable Ni remained as Ni^{2+}, then $Ni_{5/6}Mn_{1/6}(OH)_2(NO_3)_{1/6}$ or $Ni_{5/6}Mn_{1/6}(OH)_2(CO_3)_{1/12}$ could be the final product. The nitrate to carbonate ratio in the samples has been studied using CHN analysis and will be reported later below.

Figure 4 shows a schematic summary of the structures of the materials synthesized using route 1 (XRD patterns from Figure 2). The left-most structure shows the $M(OH)_2$ structure that the $Ni_xMn_{1-x}(OH)_2$ samples adopt when they are synthesized under anaerobic conditions (route 4). The next structure shows a schematic of the $x = 1$ structure, which was synthesized in air (route 1). Some Ni cations are oxidized to 3+ and anions (either nitrate or carbonate) are incorporated between some randomly selected pairs of $M(OH)_2$ slabs. The middle structure in Figure 4 shows the pure LDH phase, with turbostratically misaligned $M(OH)_2$ layers, formed when $x = 5/6$. The XRD pattern for $x = 1/2$ in Figure 2 is consistent with single $M(OH)_2$ layers. These most likely form because the sample is a two-phase mixture of LDH and Mn_3O_4, both on the nanoscale. The inclusions of nanometer-sized Mn_3O_4 would disrupt the stacking of the $M(OH)_2$ planes as is shown in the sketch for $x = 1/2$ in Figure 4. Our previous work on Co_zAl_{1-z} LDH phases showed that

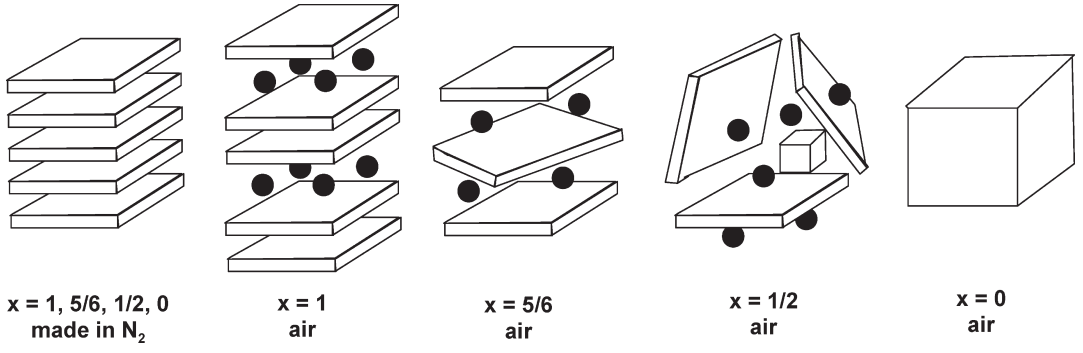

Figure 4. Schematic structures of Ni_xMn_{1-x} mixed hydroxide samples. Slabs in the diagram represent $M(OH)_2$ slabs, cubes represent Mn_3O_4 spinel, and circles represent either NO_3^- or CO_3^{2-} anions. The left-most schematic represents the $M(OH)_2$ structure that is achieved in syntheses under N_2 using route 4. Other schematics represent the products that appear during syntheses using route 1 (see text).

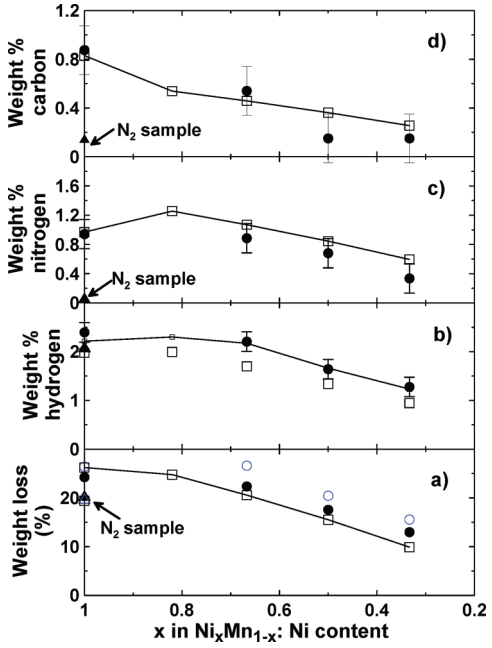

Figure 5. Chemical analysis and TGA results for Ni_xMn_{1-x} hydroxides with $x = 1$, 2/3, 1/2, and 1/3 made by route 1 and with $x = 1$ made by route 4. (a) Weight loss measured using TGA in air: ○, 30−800 °C; ●, 120−800 °C; △, route 4 sample. The □ and solid line give the calculated weight loss based on the model described in the text. (b) ●, wt % H measured by CHN analysis; large □, wt % H calculated using the model described in the text; small □ and solid line, wt % H corrected for adsorbed water. (c) ●, wt. % N measured by CHN analysis; □ and solid line, wt. % N calculated using the model described in the text. (d) ●, wt. % C measured by CHN analysis; □ and solid line, wt. % C calculated using the model described in the text. The ▲ gives the experimental data for the sample made by route 4 in all panels.

there was a limit, around $z = 0.2$, to the amount of 3+ cations that could be incorporated in the LDH phase, so this two phase description of samples for $5/6 > x > 0$ is consistent with that work.[9] Finally, when $x = 0$, the Mn_3O_4 spinel grains can grow to become large enough to give sharp diffraction peaks.

To further understand the samples prepared by route 1 and described by Figure 2, TGA and CHN analysis was made on the samples with $x = 1$, 2/3, 1/2, and 1/3. The sample with $x = 1$ made by route 4 was also studied. The solid circular data points in Figure 5 show the results of these measurements for the samples made by route 1 (in air). The solid triangular data points show the results for the $x = 1$ sample made in nitrogen using route 4.

Figure 5a shows the weight loss between 30 and 800 °C (○) and between 120 and 800 °C (●). The weight loss occurs for three reasons: (1) the loss of adsorbed or interlayer water between 30 and 120 °C, (2) the loss of interlayer NO_3^- or CO_3^{2-}, and (3) the loss of water as the hydroxides convert to oxides. Figure 5a shows that the weight loss decreases as the x, nickel content, decreases. Figure 5b shows the hydrogen content of the same samples (●) as measured by CHN analysis. The hydrogen content also decreases as the Ni content decreases. Panels c and d of Figures 5show the nitrogen and carbon content, respectively, of the samples. Both decrease as the Ni content decreases.

On the basis of the XRD results in Figure 2 and their interpretation in Figures 3 and 4, a model to describe the results in Figure 5 was developed. This model has four components: (1) The sample with $x = 1$ prepared by route 4 (under nitrogen) was assumed to be $Ni(OH)_2$ (this agrees with the diffraction pattern in Figure 2 for this sample). (2) The sample with $x = 1$ prepared in air (route 1) was assumed to be $Ni(OH)_2(NO_3)_{0.07}(CO_3)_{0.07}$ with the nitrate and carbonate amounts selected to match the CHN results. (3) The samples with $x = 2/3$, 1/2, and 1/3 were assumed to be two-phase mixtures of $Ni_{0.82}Mn_{0.18}(OH)_2(NO_3)_{0.09}(CO_3)_{0.045}$ and Mn_3O_4. (4) After heating to 800 °C, the samples converted to NiO, $NiMnO_3$, and Mn_2O_3 (depending on their initial stoichiometry) as confirmed by X-ray diffraction after TGA.

The □ in Figure 5a show the predictions of the model for the weight loss of the samples. The agreement between the model and the ● data points is quite good. The large □ in Figure 5b show the prediction of the model for the H-content of the samples. The model underestimates the amount of hydrogen in the samples. However, if hydrogen in the water released between 30 and 120 °C (from the difference between the ○ and ● in Figure 5a) is added to that predicted by the model, then the solid curve (which connects the small □ data points) in Figure 5b results. The agreement between the solid line in Figure 5b and the ● data points is very good. The comparison of the model to the experiment in panels a and b of Figure 5supports our argument that the samples are a two-phase mixture between an LDH phase (with x near 5/6) and Mn_3O_4 and the range between $5/6 > x > 0$. This assumption would lead to decreases in weight loss and H content as x decreases as observed in the experiment. Furthermore, this is consistent with the XRD observations. This is a key observation: The cation distribution within the particles for $5/6 > x > 0$ is not uniform, even though coprecipitation is used, due to the formation of Mn_3O_4 in the presence of air.

The predictions of the model for the N and C contents of the samples agree adequately as observed in panels c and d of Figure 5, respectively. We emphasize that it is beyond the scope of this paper to determine the exact ratio of carbonate to nitrate in these samples; instead, it is our aim to demonstrate that an LDH phase coexists with Mn_3O_4 for $5/6 > x > 0$ in samples prepared under oxidizing conditions (route 1).

Figure 6 shows the XRD patterns of $Ni_xMn_{1-x}(OH)_2$ samples prepared using route 4, the least oxidizing of the conditions selected. In this case, the samples with $x = 1$, 2/3, and 1/2 are pure hydroxide phases after drying in air at 80 °C. The sample with $x = 1/3$ shows more complicated behavior. Figure 6d shows the XRD pattern of the $x = 1/3$ sample directly after synthesis, while still damp. A small amount of Mn_3O_4 spinel can be observed in this XRD pattern. Figure 6e shows the XRD pattern after the 80 °C drying in air. There is almost complete conversion of the sample to the spinel phase under these drying conditions when $x = 1/3$. Figure 6 shows that excellent, single-phase hydroxides can be made for $1 > x > 1/2$ using the conditions of route 4.

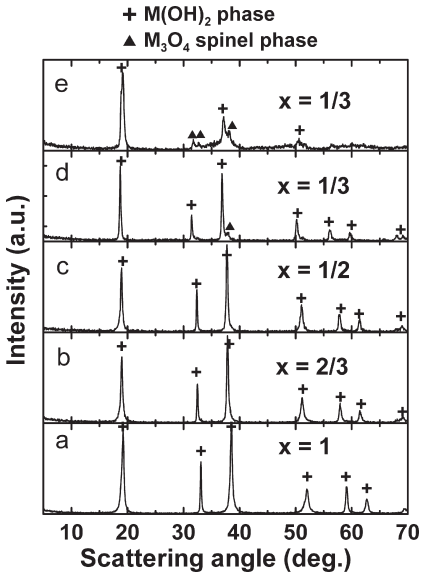

Figure 6. XRD patterns of the Ni_xMn_{1-x} mixed hydroxides with $x = 1$, 2/3, 1/2, and 1/3 synthesized using route 4 after drying at 80 °C in air, except for panel d, which shows the $x = 1/3$ sample measured while damp (no drying).

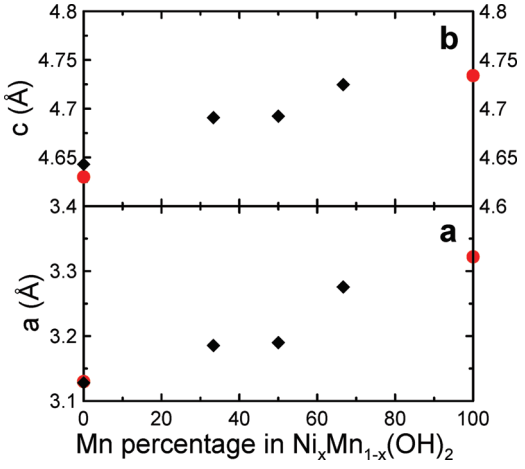

Figure 7. Lattice constants a (a) and c (b) of the $Ni_xMn_{1-x}(OH)_2$ with $x = 1$, 2/3, 1/2, 1/3, and 0 (black ◆, experimental data for samples made using through route 4; red ●, ICDD literature data).

Figure 7 shows variation of lattice constants, a and c, with the Mn content in the $Ni_xMn_{1-x}(OH)_2$ mixed hydroxides synthesized using route 4 as well as standard lattice constant values of $Ni(OH)_2$ and $Mn(OH)_2$ (red ●) from the International Center for Diffraction Data. With an increase in Mn content from 0% to 100%, lattice constant, a, increases from around 3.130 to 3.322 Å, and lattice constant, c, increases from around 4.630 to 4.734 Å. The smooth variation in lattice constants with composition also indicates that pure single phase $Ni_xMn_{1-x}(OH)_2$ has been prepared using route 4.

Figure 8 shows XRD patterns of targeted $Ni_xMn_{1-x}(OH)_2$ samples with $x = 2/3$ and $x = 1/2$ made using routes 1, 2, 3, and 4. The exposure of the samples to oxygen decreases from route 1 to 4. This is evident from the phases observed in the XRD patterns. For example, Figure 8a shows a mixture of LDH and nanosized Mn_3O_4 spinel (as argued above). Figure 8b (route 2) shows LDH and a small amount of hydroxide. Figure 8c (route 3) shows less LDH and more hydroxide. Finally, Figure 8d (route 4) shows a pure hydroxide phase. The same trends in diffraction patterns are observed for the $x = 1/2$ samples prepared by routes 1−4 as shown in panels e−h of Figures 8. The results in Figure 8 clearly show that researchers must pay attention to the hydroxide synthesis route when both Ni and Mn are included. Synthesis by route 3 can be used to prepare predominantly pure $Ni(OH)_2$ (not shown), but route 3 fails when Mn is added. If it is a goal to prepare mixed Ni−Mn hydroxides with a homogeneous cation distribution, then Figure 8 shows that air must be excluded from the synthesis when Mn is present. Otherwise two-phase products, where the Ni and Mn content differs between the phases, will result. Such precursors may be problematic for the production of lithium transition metals oxides with homogeneous cation distribution.

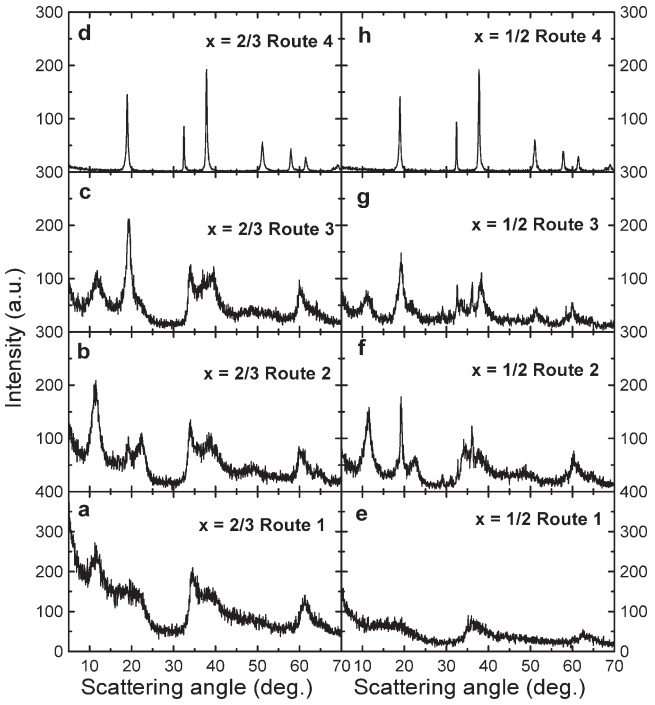

Figure 8. XRD patterns of samples with $x = 2/3$ and $x = 1/2$ made using routes 1−4 as indicated in the panels. The exposure of the samples to oxygen during synthesis and drying decreases from route 1 to 4.

Figure 9 shows SEM images of $Ni_{2/3}Mn_{1/3}(OH)_2$ samples synthesized by routes 1−4. The products of route 1−3 show no regular morphology, and the particle size varies wildly. This particle size is set by the size of aggregates produced during the gentle grinding of the dried product. By contrast, the samples produced by route 4 are made up of spherical particles with a mean size of about 10 μm and relatively narrow size distribution (Figure 9d). Panels e and f of Figure 9show an enlarged view of a single spherical particle. The spherical particle is made up of smaller primary platelike particles with a thickness of around 200 nm and length of around 1−2 μm. The formation of the dense spherical particles is due to the ammonia-induced dissolution−recrystallization

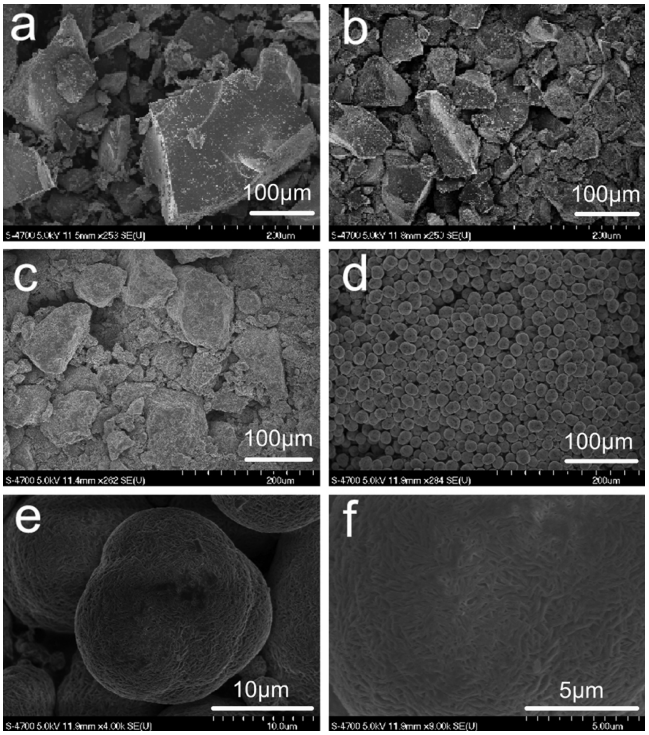

Figure 9. (a−d) SEM images of the $Ni_{2/3}Mn_{1/3}$ mixed hydroxide samples synthesized by routes 1− 4, respectively. (e, f) Enlarged SEM images of the $Ni_{2/3}Mn_{1/3}$ mixed hydroxide synthesized using route 4.

process of the initially precipitated mixed hydroxide nanoparticles because of their strong tendency to minimize their surface energy.[17,18]

(17) van Bommel, A.; Dahn, J. *J. Electrochem. Soc.* **2009**, *156*, A362.
(18) van Bommel, A.; Dahn, J. Chem. Mater., in press.

The results presented above demonstrate that it is possible to prepare excellent single phase $Ni_xMn_{1-x}(OH)_2$ samples that are dense and spherical. In order to do so, attention must be paid to the amount of oxygen the samples are exposed to during the coprecipitation reaction and to the details of the ammonia content, temperature, and pH of the reaction.[17,18]

Conclusions

$Ni_xMn_{1-x}(OH)_2$ mixed hydroxide intermediates with $x = 1, 5/6, 2/3, 1/2$, and $1/3$ were prepared by four different coprecipitation routes and studied by XRD, chemical analysis, and SEM techniques. The results of these studies show that when air is present during the coprecipitation reaction a series of complex structures that include layered double hydroxide (LDH) and Mn_3O_4 phases are formed. Elimination of air during synthesis leads to excellent single-phase $Ni_xMn_{1-x}(OH)_2$ samples. Ammonia, pH control, and elevated temperature can be used to produce dense and spherical hydroxide $Ni_xMn_{1-x}(OH)_2$ particles as shown in the literature.[17,18]

If it is a goal to prepare mixed Ni−Mn hydroxides with a homogeneous cation distribution, then air must be excluded from the synthesis when Mn is present. Otherwise two-phase products where the Ni and Mn content differs between the phases will result. Such precursors may be problematic for the production of lithium transition metals oxides with homogeneous cation distribution.

Acknowledgment. The authors acknowledge the financial support of NSERC and 3M Canada.